

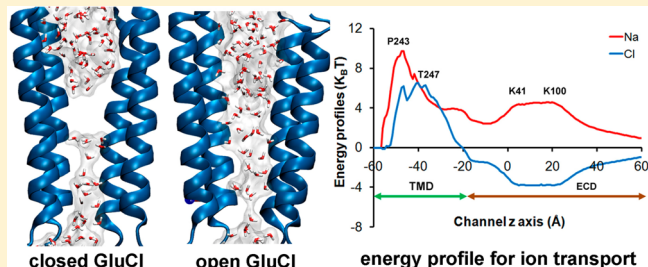
Energetics and Ion permeation Characteristics in a Glutamate-Gated Chloride (GluCl) Receptor Channel

Mary Hongying Cheng[†] and Rob D. Coalson*

Department of Chemistry, University of Pittsburgh, Pittsburgh, Pennsylvania 15260, United States

Supporting Information

ABSTRACT: An invertebrate glutamate-gated chloride channel (GluCl) has recently been crystallized in an open-pore state. This channel is homologous to the human Cys-loop receptor family of pentameric ligand-gated ion channels, including anion-selective GlyR and GABAR and cation-selective nAChR and SHT₃. We implemented molecular dynamics (MD) in conjunction with an elastic network model to perturb the X-ray structure of GluCl and investigated the open channel stability and its ion permeation characteristics. Our study suggests that TM2 helical tilting may close GluCl near the hydrophobic constriction L254 (L9'), similar to its cation-selective homologues. Ion permeation characteristics were determined by Brownian dynamics simulations using a hybrid MD/continuum electrostatics approach to evaluate the free energy profiles for ion transport. Near the selectivity filter region (P243 or P-2'), the free energy barrier for Na⁺ transport is over 4 $k_B T$ higher than that for Cl⁻, indicating anion selectivity of the channel. Furthermore, three layers of positivity charged rings in the extracellular domain also contribute to charge selectivity and facilitate Cl⁻ permeability over Na⁺. Collectively, the charge selectivity of GluCl may be determined by overall electrostatic and ion dehydration effects, perhaps not deriving from a single region of the channel (the selectivity filter region near the intracellular entrance).



INTRODUCTION

Members of the pentameric ligand-gated ion channel (pLGIC) superfamily share considerable structural similarity. Each receptor channel of this type contains five subunits that form a pentameric channel pore that conducts cations or anions. Human pLGICs mediate neurotransmission and are sometimes referred to as the Cys-loop receptor family due to conserved disulfide bonds in the extracellular domain. Cys-loop receptors include cation-selective nicotinic acetylcholine receptors (nAChRs) and serotonin receptors (SHT₃), as well as anion-selective glycine receptors (GlyRs) and GABARs. It has been proposed that charge selectivity of pLGICs is determined by the selectivity filter region in the transmembrane (TM) domain near the intracellular entrance: a GLU residue (i.e., E-1' in nAChRs and SHT₃) for selective cation permeation and an ALA (i.e., A-1' in GlyRs and GABARs) residue for anion permeation.¹ The overall effective charge near the intracellular entrance is critical for the charge selectivity.² In this region a basic residue (R0' or K0') is conserved and the tunable charge state of this residue is suggested to be associated with charge selectivity in pLGICs.³ Furthermore, the pore constriction of the selectivity filter region also contributes to selective ion permeation.^{4–6} In addition to the selectivity filter region in the TM domain, a series of charged rings in the extracellular (EC) domain has been suggested to play an important role to channel conductance and charge selectivity.⁷

The X-ray crystal structures of the cation-selective bacterial *Gloeobacter vioaceus* pentameric ligand-gated ion channel

(GLIC)^{8,9} shows that GLU residues (E-2') line the intracellular entrance, thereby supporting the association of negatively charged residues with cation permeation.¹ Very recently, an invertebrate glutamate-gated chloride channel (GluCl) has been crystallized in an open-pore state.⁴ GluCl is the first X-ray structure of an anion-selective pLGIC in an open-pore state, and thus provides an important structural starting point for modeling ion permeation through such channels, and for learning more about the physicochemical determinants of charge selectivity as well as gating and other aspects of open channel stability in this important channel class. The atomic structure of the open GluCl⁴ was iteratively refined on the basis of an initial homology model of GluCl constructed from the cation-selective pLGIC protein GLIC.^{8,9} Although the GLIC model was initially assumed to be a representative open-channel model,^{8,9} recent experimental studies suggest that the open GLIC model is perhaps best characterized as a closed-channel state corresponding to channel desensitization.^{10,11} Indeed, MD simulations of the GLIC protein^{12–14} have demonstrated that the GLIC channel cannot sustain a long time open state conformation: the channel spontaneously closed on a time scale of tens of nanoseconds. This raises concerns regarding the open channel stability of these pLGICs,

Received: July 28, 2012

Revised: September 26, 2012

and hence on the reliability of previously proposed open state structures.

To address these concerns, in the present study we used elastic network model (ENM)¹⁵ together with molecular dynamics (MD) simulations to perturb the X-ray crystal structure of GluCl. In particular, the lowest frequency eigenvector corresponding to the twist mode¹⁶ was used to expand the channel pore of the GluCl protein, following an established procedure.^{17,18} For the pLGICs, this twist motion has been suggested as a major motion associated with the channel gating.^{9,16,19} Interestingly, the ENM-perturbed GluCl protein that we constructed remained in an open-channel state during the entire 100 ns of MD simulations. In contrast, the GluCl protein from the crystal structure dehydrated near the hydrophobic constriction L254 (L9') on a time scale of tens of nanoseconds. Given a stable open channel structure, we employed a hybrid MD/Brownian dynamics (BD) approach to investigate the ion permeation characteristics in the ENM-perturbed GluCl protein. Our calculations demonstrate that the GluCl is anion-selective with a channel conductance more than four times smaller than GLIC.

METHODS

Preparation of Simulation Systems. Two computational models of the GluCl receptor were constructed for MD investigation: namely, (1) X-GLUCl, in which GluCl protein with five bound glutamate agonist molecules was obtained from the crystal structure of GluCl-Fab complex (PDB: 3RIF) by stripping out the allosteric agonist ivermectin and other material; (2) ENM-GLUCl, for which the lowest frequency eigenvector (corresponding to the twist mode¹⁶) obtained from an elastic network model (ENM),¹⁵ was used to perturb the X-ray crystal structure of the GluCl protein. The initial structure of the ENM-GLUCl system was generated through two cycles of small displacements followed by local minimization on the CHARMM potential energy surface²⁰ according to^{17,18} $R(\pm) = R^0 \pm s\lambda^{-1/2}\mu$, where R and R^0 are the instantaneous and original (or previous cycle) 3N-dimensional vectors of atomic coordinates (N being the number of atoms), respectively, λ and μ are the lowest frequency (twist mode) eigenvalue and eigenvector, respectively, and s is an amplification factor used to expand/contract the channel pore in the transmembrane domain.

The protonation state of titratable residues of GluCl was estimated on the basis of the pK_a calculations carried out using PROPKA.²¹ Default charges²⁰ were assigned to all titratable residues except E293, for which a neutralized charge state was assigned because this residue was embedded in a highly hydrophobic environment and the estimated pK_a value was ca. 8.7. The TM domain of the GluCl was inserted into the center of a cylinder of pre-equilibrated POPC lipid. The outer radius of the cylinder POPC lipid construct is approximately 52.3 Å. Fully equilibrated TIP3 waters were added to the system to generate hexagonal boundary conditions of 104.6 Å × 104.6 Å × 135 Å. Na⁺ and Cl⁻ ions corresponding to a 0.15 M solution were added to neutralize the system. There were one GluCl, 179 POPC, 41 Cl⁻ ions, 31 Na⁺ ions, and about 25 400 water molecules for a total of over 130 000 atoms. Figure 1 shows the setup of the MD simulation system.

Molecular Dynamics Simulations. MD simulations were performed using the NAMD2 program.²² The CHARMM force field with CMAP corrections was used for protein, water, and lipids.^{20,23} The two channel protein models were subjected to

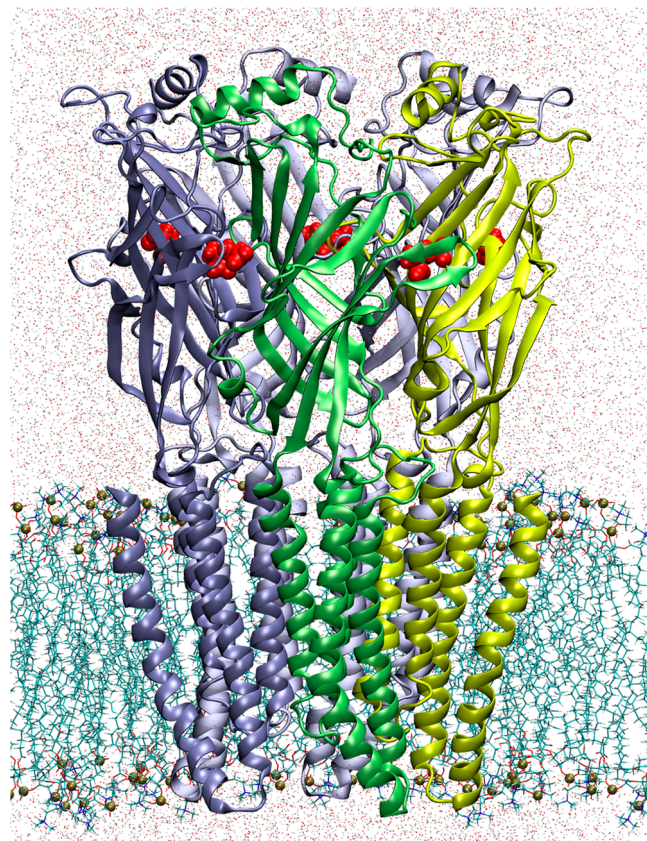


Figure 1. Representative MD setup of the GluCl protein embedded into fully solvated POPC lipids (in line format). Phosphorus atoms are shown as tan spheres. Red VDW balls represent glutamate ligands. Water molecules are shown as dots.

the same simulation procedure. The system was first energy minimized for 50 000 steps. Then it underwent 0.5 ns constant volume and temperature ($T = 310$ K) (NVT) simulation and subsequent 4 ns Nosé–Hoover constant pressure ($P = 1$ bar) and temperature ($T = 310$ K) (NPT) simulation, during which the protein was fixed and the constraint on the POPC head groups was gradually released to zero. Subsequently, the constraint on the GluCl backbone was gradually reduced from 10 kcal/mol to zero within 3 ns. Finally, the unconstrained protein underwent NPT simulation for 100 ns in the ENM-GLUCl system and 50 ns in the X-GLUCl system. The simulation protocol included periodic boundary conditions, water wrapping, hydrogen atoms constrained via SHAKE, and long-range electrostatic forces evaluated via the particle mesh Ewald (PME) algorithm.²⁴ The bonded interactions and the short-range nonbonded interactions were calculated every time step (2 fs) and every two time-steps (4 fs), respectively. Electrostatic interactions were calculated at every four time-steps (8 fs). The cutoff distance for nonbonded interactions was 12 Å. A smoothing function was employed for the van der Waals interactions at a distance of 10 Å. The pair-list of the nonbonded interactions was calculated every 20 time-steps with a pair-list distance cutoff of 13.5 Å.

Brownian Dynamics Simulations. Brownian dynamics (BD) calculations of ion permeation characteristics were carried out using a dynamic Monte Carlo (DMC) algorithm. A detailed description of the algorithm can be found in refs 25–27. Briefly, the protein channel, lipid bilayer membrane, and water solvent were treated as continua characterized by different dielectric

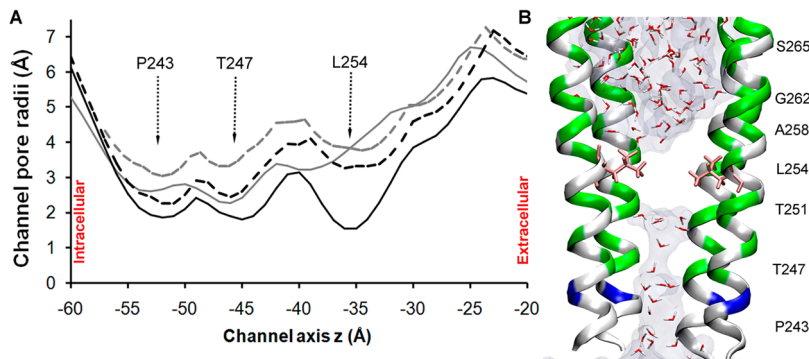


Figure 2. (A) Comparison of the channel pore radii inside the TM domains of initial structures of X-GLUCl (black dashed line) and ENM-GLUCl (gray dashed line), and the MD relaxed X-GLUCl (black line) and ENM-GLUCl (gray line) at 50 ns. The intracellular and extracellular entrances to the TM domain are marked. (B) Discontinuous water occupancy was observed near L254 (L9') in the MD relaxed X-GLUCl. For clarity, only four TM2 segments are shown. Green, white, and blue represent hydrophilic, hydrophobic, and positively charged residues, respectively.

constants, but ions were treated explicitly, undergoing 3D Brownian motion according to the following effective potential:

$$W_k = \phi_k^{\text{mem}} + \phi_k^{\text{PMF}} + \sum_{j \neq k} \frac{q_k q_j}{\epsilon_w} \phi^{\text{coul}}(r_{kj}) + \sum_{j \neq k} q_k q_j \phi_{kj}^{\text{diel}} - k_B T \ln(D(z)/D_0) \quad (1)$$

where q_k and q_j are the charges of ion k and j , respectively, and D_0 and $D(z)$ are the diffusion constants of an ion in the bulk and at position z , respectively. The first term in the right-hand side of eq 1 is an externally applied transmembrane potential, which was calculated by solving Poisson's equation for the 3D channel/membrane geometry and imposing the applied voltage V on the boundary of the computational electrostatics box (i.e., specifying a potential V on the internal face of the computational box and a 0 potential on the external box face).^{25,28} The second term is the energy profile for single ion transport calculated using a hybrid MD/continuum approach,²⁶ which combined all-atom MD calculations of the potential of mean force (PMF) in the narrow TM domain region of the channel with an approximate electrostatics/dielectric continuum model evaluation of the same quantity in the large pore regions (for details see Supporting Information). The third and fourth terms together account for long-ranged Coulombic ion-ion interactions in a dielectric inhomogeneous medium, which were estimated following a previously developed approach.^{18,25,29} The last term is introduced to account for the spatial dependence of the ion diffusion constant in Brownian dynamics simulations.^{27,30} A hard-core excluded volume potential (not explicitly indicated in eq 1) was also included in the BD simulation algorithm. In particular, any overlap between an ion and the protein/membrane or between any two ions was not permitted. For each specified applied voltage, a total of 8 independent BD simulations were carried out with each run lasting 22.4 μ s. Radii of 1.8 and 0.95 Å were taken for Cl⁻ and Na⁺, respectively. As was done in our previous calculations of the homologous GLIC channel,²⁶ diffusivities for Na⁺ and Cl⁻ were taken to be 1.33×10^{-5} and 2.02×10^{-5} cm²/s in bulk water,³¹ then reduced from their bulk values near the receptor entrances to 0.3 times these values near the TM entrances, and maintained at 0.3 times of their bulk values throughout the entire TM region.

Adaptive Biasing Force Calculations. The single ion potential of mean force (PMF) (ϕ_k^{PMF} in eq 1 of the text) for transporting Na⁺ or Cl⁻ through the transmembrane (TM)

pore region of the ENM-GLUCl was carried out using the adaptive biasing force (ABF)^{32,33} method implemented in NAMD.²² Briefly, ABF calculations of the PMF were carried out in eight different windows along the channel z axis (perpendicular to the membrane lipids). The width of each ABF window was 5 Å and two or three consecutive 2 ns ABF calculations were performed for each window, resulting in a total of 42 ns ABF calculations. The initial structure for the PMF calculations was taken from an MD snapshot after 20 ns simulation of ENM-GLUCl and the configuration for each ABF window was obtained from an additional 300 ps equilibration simulation that had the target ion positioned within the window. Following a previously utilized approach,^{26,34} within each window the average force acting on the target ion was accumulated in 0.1 Å sized bins. The boundary force constant was set to be 10 kcal/mol. The biasing force was applied only after the accumulation of 800 samples in individual bins.

Data Analysis. Radii of the model channels were measured using the HOLE program.³⁵ VMD³⁶ was used to analyze important channel features, such as the root-mean-square deviation (RMSD), the average pore radii, TM2 helical tilting angles, etc. For structural averaging calculations, each frame from MD was aligned with the initial model before determination of an average structure. The standard deviation for the ABF-calculated PMF was estimated from different runs and also from simulations of different lengths.

RESULTS

Structural Stability and Variability. The stability of our model channels was assessed via the $C\alpha$ root-mean squared deviation (RMSD) of the protein structure from the X-ray structure of GluCl. Results are shown in Figure S1 (Supporting Information). The RMSD for the whole receptor of X-GLUCl stabilized at ca. 2.5 ± 0.2 Å within 15 ns of MD simulation and remained nearly constant during the subsequent 35 ns simulations. The stabilized RMSD for the TM domain of X-GLUCl was only 1.6 ± 0.1 Å. For ENM-GLUCl, the RMSD of the initial model deviated by ca. 1.2 Å from that of the X-ray structure of GluCl. Similar to that for X-GLUCl, the RMSD of ENM-GLUCl showed a nearly flat plateau of ca. 2.5 ± 0.2 Å after 15 ns MD simulation. In contrast to the X-GLUCl system, the TM domain of ENM-GLUCl displayed a similar degree of deviation as found for the whole receptor. Overall, the RMSDs for ENM-GLUCl (calculated from 15 to 100 ns) were 2.63 ± 0.23 and 2.34 ± 0.18 Å for the whole receptor and TM domain,

respectively, and slight increases of 0.30 ± 0.15 and 0.25 ± 0.10 Å were observed within the last 40 ns simulations for the whole receptor and TM domain, respectively.

Despite the similar RMSDs, different structural variations and degrees of channel dehydration were observed in these two models. Near the intracellular entrance (P243 to T251), the MD-equilibrated pore radii in the X-GLUCl model were contracted from their X-ray structure value by an average of 0.4 Å, and significant pore reduction occurred near the hydrophobic constriction L254 (L9'), in which the pore radius decreased from 3.3 Å (in the X-ray structure) to 1.8 ± 0.3 Å (cf. Figure 2A). Discontinuous water occupancy near the hydrophobic constriction L254 (L9') position (Figure 2B) occurred intermittently after 20 ns of MD simulation, indicating that MD relaxation of the X-GLUCl resulted in a putative closed channel state. Dehydration of the channel pore is implicated as a symptom of channel closure as previously observed in MD simulations of the homologous cation-selective GLIC.^{12–14} Channel dehydration has been found to be associated with tilting of the TM2 helices.^{12,13} Following a previously introduced approach,^{12,37} we calculated the TM2 helical tilting angles along the radial and lateral direction. Compared to the X-ray crystal structure, the averaged radial tilting angle was reduced from 6.25° to $5.25 \pm 0.5^\circ$, and the lateral tilting angles from 3° to $1.0 \pm 0.5^\circ$ after 50 ns MD simulation of X-GLUCl. Consistent with a previous investigation of channel closure in cation-selective GLIC,¹² the reduction in the TM2 helical tilting angles was also observed to induce channel dehydration in the anion-selective GluCl, suggesting that pLGICs may share a common gating mechanism.

In contrast to the X-GLUCl system, continuous water fully occupied the ENM-GLUCl channel pore during the entire 100 ns MD simulation. Inside the TM domain of the initial ENM-GLUCl, the pore radii expanded by an average of 0.5 Å (Figure 2A), whereas the pore radii in the extracellular domain were almost identical (not shown). In the first 50 ns MD simulations, the channel pore radii near the intracellular entrance (P243 to T251) fluctuated within 0.3 Å around the X-ray crystal structure; near the hydrophobic constriction L254 (L9'), the pore radius enlarged from 3.3 Å (X-ray) to 3.9 ± 0.4 Å within the first 20 ns of MD simulation, and then remained almost unchanged for more than 30 ns. At ca. 50 ns of simulation time, the hydrophobic constriction near L254 underwent further enlargement to 5.0 ± 0.4 Å over a 10 ns time scale, and remained stable at this pore radius for the subsequent 40 ns of MD simulation.

Energy Profiles for Ion Transport. Following our previously employed approach,²⁶ we calculated the single ion PMF for transporting Na^+ or Cl^- through the transmembrane (TM) pore region of the ENM-GLUCl using the ABF method.^{32,33} The initial protein structure for the ABF calculations was taken from a snapshot of the ENM-GLUCl which had been relaxed for 20 ns, which was chosen as the working structure for estimation of ion permeation characteristics because this structure represents a stabilized channel (upon which meaningful equilibrium MD calculations can be performed) that is reasonably close to the open-pore X-ray structure.

ABF calculations of the PMF started from the intracellular entrance and were carried out in eight windows along the ion transport direction (the channel z axis) (cf. Figure 3A). Each window had a width of 5 Å and for each window three consecutive 2 ns ABF calculations were performed. The

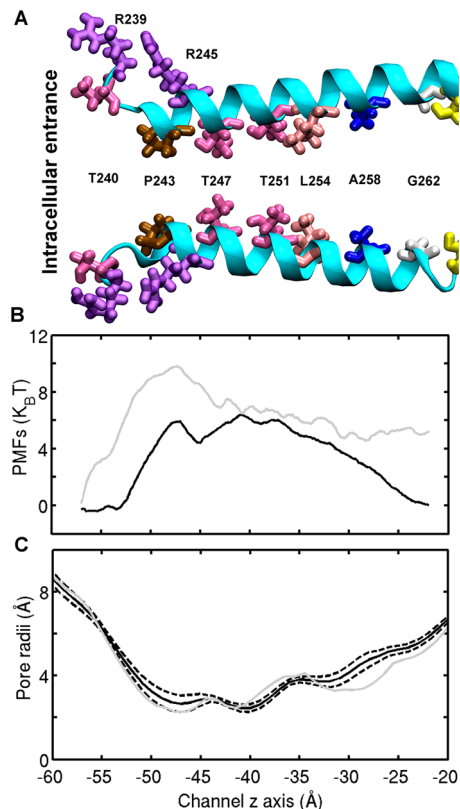


Figure 3. (A) Schematic depiction of the pore lining TM2 segments. (B) Comparison of PMFs for transporting a Cl^- (black line) or Na^+ ion (gray line) through the transmembrane domain pore of the ENM-GluCl. (C) Comparison of the channel pore fluctuation with the X-ray crystal structure. The gray line shows the radius profile of the crystal structure. The black line represents the radius profile averaged over different windows for both Na^+ and Cl^- and the two dashed lines delineate the standard deviation about the mean value.

calculated PMFs converged within 6 ns (specifically, the variation of the PMF at any point along the z-axis was less than 1 kcal/mol within two consecutive runs). During the 6 ns ABF calculations, the maximum channel pore radii fluctuations were less than ± 0.4 Å, estimated over all calculations in different windows (Figure 3C). Overall, the majority of pore radii fluctuation is less than 0.4 Å about the X-ray crystal structure, indicating that the PMF calculations reasonably reflected the free energy profiles for ion transport through the putative open GluCl channel.⁴ Near the charge selectivity filter region (P243 to T247),⁴ Na^+ and Cl^- experienced energy barriers of ca. 10.0 ± 2.0 and $6.1 \pm 1.5 k_{\text{B}}T$, respectively (Figure 3B). These energy barriers to ion transport are caused primarily by pore constriction in this region ($\sim 2.4 \pm 0.4$ Å), which results in partial stripping of the hydration shell carried by Na^+ and Cl^- . Near the intracellular entrance, long ranged electrostatic interactions from R239 and R245 (Figure 3A) may assist in attracting Cl^- over Na^+ and contribute partially to the enhancement of Cl^- permeability over that of Na^+ . Furthermore, positive electrostatic potential due to the protein backbone dipole may also facilitate Cl^- permeation.⁴

In recent work, we demonstrated the utility of a simple method for combining high-resolution all-atom MD simulation based ion free energy profiles in the narrow TM domain region of an ion channel with lower resolution (but much faster) continuum electrostatics based calculations of the same

quantities in the wider vestibular region of the channel.²⁶ Adopting this hybrid approach, we calculated the energy profiles for single ion transport through the entire GluCl (Figure 4). Near the intracellular entrance to the TM domain,

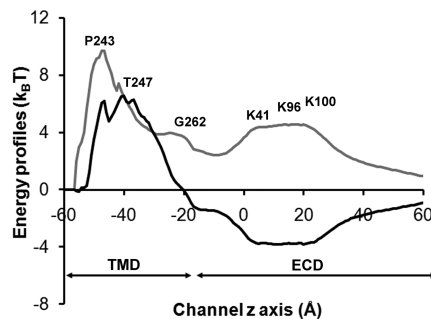


Figure 4. Comparison of free energy profiles for transporting a Cl^- (black) and Na^+ ion (gray) along the channel center line of the ENM-GLUCl model channel in the absence of an external membrane potential. A hybrid MD/continuum strategy was implemented to estimate the single ion PMF for transporting a Na^+ or Cl^- ion in BD simulations. The z position at which the MD and continuum electrostatics PMFs were joined was chosen to be $z = -22 \text{ \AA}$ (near G262). For simplicity, the free energy profiles for both Cl^- and Na^+ are assumed to be identically zero in the intracellular region, $z < -58 \text{ \AA}$.

both Na^+ and Cl^- were assumed to have the same free energy value of $0 \text{ } k_{\text{B}}T$. This point is already in the internal solution and the PMF function does not change much if integrated out further into the internal solution region. From the extracellular entrance to the TM domain, the ABF-based 1D PMF was connected with 3D continuum-based energy profiles near G262, where the lateral variations in the 3D energy profile were small ($\sim 1 \text{ } k_{\text{B}}T$) for permeant ions, thus allowing for a 3D electrostatic energy profile to be treated as a 1D PMF without sacrificing much computational accuracy.²⁶ Collectively, our hybrid free energy calculation suggests that GluCl is anion-selective and that the anion selectivity is determined not only by a $4 \text{ } k_{\text{B}}T$ lower energy barrier for Cl^- vs Na^+ transport through the intracellular entrance but also by an energy well ($-4 \text{ } k_{\text{B}}T$ for Cl^- compared to $4 \text{ } k_{\text{B}}T$ for Na^+) experienced by Cl^- in the extracellular domain.

Ion Permeation Characteristics. Ion permeation characteristics in the GluCl were calculated via BD simulations (see Methods) of ion transport through the MD relaxed ENM-GLUCl model channel, employing single ion free energy profiles calculated via the aforementioned hybrid MD/continuum approach. The current–voltage (I – V) relationship at the single-channel level was obtained from BD simulations of symmetrical 0.15 (M) NaCl in both extracellular and intracellular solutions. The result is shown in Figure 5. Our simulations yielded a linear I – V relationship over a range of applied external potential from -60 to $+60$ mV. This linear current–voltage relationship broadly agrees with the whole-cell current measurement over the same voltage range (cf. Supplemental Figure 20 in ref 4). Furthermore, our calculations predict that this linear I – V relationship breaks down as the externally applied membrane potential is increased (i.e., $>+80$ mV or <-80 mV) (see Figure S2, Supporting Information). In particular, the current increases in a superlinear fashion at high membrane potentials of either parity. The simulated currents (I) at different applied voltage (V) were collected, and the conductance was calculated as the slope of the linear least-

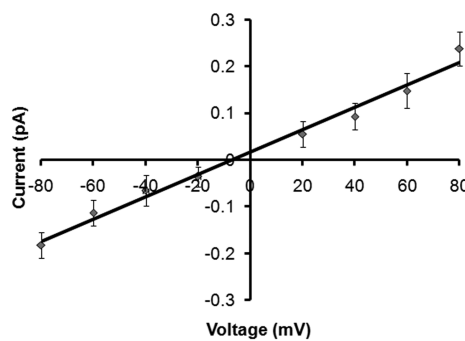


Figure 5. BD simulated current–voltage relationship in the ENM-GLUCl model channel. BD data points are shown as diamonds with error bars. The solid line shows a linear least-squares fit to the simulation data. These BD simulations were carried out in symmetric bathing solutions of 0.15 M NaCl. The calculated channel conductance (slope of the least-squares fit I – V curve) is $2.0 \pm 0.5 \text{ pS}$, and the reversal potential is $-7.5 \pm 1.5 \text{ mV}$.

squares curve fit to the I – V data points in Figure 5. The single channel conductance calculated by our BD simulation was $2.0 \pm 0.5 \text{ pS}$ (calculated over the applied voltage range -80 to $+80$ mV), which is almost 4 and 40 times smaller than that found in the cation-selective GLIC⁹ and ELIC,³⁸ respectively. The pore constriction inside the selectivity filter region ($\sim 2.6 \text{ \AA}$) and the absence of positively charged residues lining the TM pore may contribute to the comparatively low single channel conductance in GluCl. The reversal potential (at which the total electric current is zero) obtained in our BD simulations under symmetric bathing solution (0.15 M) conditions was $V_{\text{res}}^{\text{sym}} = -8.0 \pm 1.5 \text{ mV}$, corresponding reasonably well to the reversal potential of -10.0 mV observed in the whole-cell current measurements.⁴

The simulated current ratio $I_{\text{Cl}}/I_{\text{Na}}$ depended on the applied membrane potential. We found $I_{\text{Cl}}/I_{\text{Na}} > 10$ under positive membrane potentials (when Cl^- transports from the extracellular to intracellular side), which was more than 3 times larger than the ratio $I_{\text{Cl}}/I_{\text{Na}} < 3$ we obtained under negative membrane potentials (when Cl^- transports from the intracellular to extracellular side). The difference may originate from the energetics governing ion transport: near the intracellular entrance to the TM domain, both Cl^- and Na^+ experience energy barriers due to the pore constriction (cf. Figure 4); inside the extracellular domain, a series of positively charged rings concentrates Cl^- relative to its value in bulk solution, and thus facilitates Cl^- permeation from the extracellular domain.

To date, no experimental single channel measurement has been performed on GluCl. Thus we compared our results with the selectivity ratio obtained in its anion-selective homologues. For GlyR, the experimentally measured permeability ratio $P_{\text{Cl}}/P_{\text{Na}}$ is 24 ± 3 ,^{5,39} which is 2–8 times larger than that calculated in GluCl by our BD simulations. Whereas there exists some difference between the experimental method (based on reversal potential) and the computational method (direct calculation of ion current) used to estimate the selectivity ratio, possible structural variations near the selectivity filter region in different anion-selective channels are also worth noting, as these may have some effect on channel conductance. In GlyR, mutations in R0' did not generate any functional channels,⁴⁰ but mutants of an $\alpha 7$ -GluCl/ β chimera⁴¹ and $\rho 1$ GABAR² at the homologous

R0' position not only functioned but also showed moderate reduction in the selectivity ratio of Cl^- over Na^+ .

■ DISCUSSION

We observed in MD simulations that the anion-selective GluCl channel was able to close near the hydrophobic constriction L254 (L9'), which is broadly consistent with the gate position proposed for other pLGICs.^{1,6,42,43} Furthermore, similar variations in the TM2 helical tilting angles were found to induce channel closure in both GluCl and the cation-selective GLIC.¹² This suggests that both cation-selective and anion-selective pLGICs may share similar hydrophobic gates at the 9' position. The closing of X-GLUCI in our simulation may be induced by two features: (i) absence of ivermectin and/or (ii) intrinsic closing tendency, as was observed in the homologue GLIC receptor following a similar simulation protocol.¹² In future simulations, inserting ivermectin into its binding sites as identified in the X-ray structure will help us to understand the channel gating and potentiation mechanisms of pLGICs.

Compared to the X-ray crystal structure of GluCl, the pore radius near the hydrophobic constriction L254 of our open-channel GluCl (ENM-GLUCI) was larger: Near L254, the channel pore radius was enlarged from 3.3 Å (X-ray) to 3.9 ± 0.4 Å (which remained stable for more than 30 ns), and finally to 5.0 ± 0.4 Å (which remained stable for the last 40 ns of MD) (cf. Figure S3, Supporting Information). The increase of the pore radius was mainly due to the local reorientation of the side chains of TM2 segments together with an overall backbone expansion of 0.5 ± 0.15 Å in the TM channel pore. The structural variation in the simulations may be due to the lack of stabilization by ivermectin.⁴ It may also reflect dynamical variations of the open channel structure, as evidenced by the fluctuations in open channel currents that typify electrophysiological measurements.^{3,5,39}

The precise meaning of these multiple comparatively stable hydrated channel pore conformations observed in our MD simulations is unclear: perhaps they are associated with multiple open channel states (resulting in multiple conductances) observed in other pLGICs (e.g., GlyR has five distinguishable conductances¹). In our simulations, this pore enlargement transition was associated with an increased exposure of T255 (T10') to the channel lumen due to expansion of the pore. To check our theoretical findings, experimental studies of the accessibility of cysteine mutants introduced into the TM2 domain would be useful. Our simulations imply that the accessibility of T10' may be state-dependent and there is increased T10' accessibility as the channel goes from closed to open states (especially the state with an enlarged pore radius of 5.0 ± 0.4 Å near L254).

Using a combined computational, structural, and electrophysiological approach, Sine et al.⁷ observed that in the cation-selective nAChR, a series of negatively charged residues in the extracellular domain contributed significantly to the channel conductance and charge selectivity. Similarly, we found that in the EC domain of the anion-selective GluCl, three layers of positively charged residues (K41, K96, and K100) generated an electrostatic energy well for Cl^- (Figure 4) and thus may facilitate Cl^- permeation over Na^+ . In contrast, both Cl^- and Na^+ evidenced energy barriers near the selectivity filter region of GluCl. However, the energy barrier for Na^+ is higher than Cl^- , thus favoring anion-selective permeation. Taken together, our theoretical study suggests that the charge selectivity of GluCl may be determined by overall electrostatic and ion

dehydration effects, perhaps not originating from a single region of the channel, namely, the selectivity filter region near the intracellular entrance.

■ CONCLUSIONS

High resolution crystal structures provide invaluable structural bases for understanding the ion transport characteristics of ion channels. For ion transport through a narrow channel pore, protein dynamics and the hydration state of a permeant ion may significantly affect the energetic of ion permeation. These effects may not be accurately captured by a static protein structure but can, in fact, be assessed by atomic MD calculations of the single ion PMF. Nevertheless, due to the existence of multiple channel states, MD relaxation often results in closed-channel states,^{12,14} thus raising concerns about the open channel stability. Here we demonstrate that adjustment of the channel structure using an elastic network model (ENM)^{15,44} in conjunction with MD simulations¹⁸ can significantly improve the open channel stability of GluCl. Our MD-relaxed ENM-GLUCI remains fully hydrated over the entire 100 ns MD simulation interval, characterized by pore radii fluctuation within 0.4 Å of the X-ray structure in the majority of the channel pore. Near the hydrophobic constriction (L254), an enlarged pore (more than 0.5 Å larger than that in the X-ray structure) prevents the channel from dehydration and assists in preserving an open-channel state.

Our BD simulations reveal that both Cl^- and Na^+ can transport through GluCl, with the permeability of Cl^- being 3–11 times higher than that of Na^+ . The permeability ratio of Cl^- over Na^+ , obtained here as the simulated current ratio $I_{\text{Cl}}/I_{\text{Na}}$, depends on the applied membrane potential. A higher ratio of $I_{\text{Cl}}/I_{\text{Na}}$ is observed when Cl^- transports from the extracellular to the intracellular side. We emphasize that rings of positively charged pore lining residues in the extracellular domain, in addition to the region of the proposed selectivity filter region,⁴ may contribute to the charge selectivity and channel conductance in GluCl.

■ ASSOCIATED CONTENT

Supporting Information

Details of continuum calculation of electrostatic potential. Supporting results mentioned in the text, including figures of the comparison of backbone RMSD from the X-ray structure (Figure S1), current–voltage relationship (Figure S2), and comparison of channel pore radii (Figure S3). Complete author list for ref 20. This material is available free of charge via the Internet at <http://pubs.acs.org>.

■ AUTHOR INFORMATION

Corresponding Author

*Address: Department of Chemistry, Chevron Science Center, 219 Parkman Ave., Pittsburgh, PA 15260. E-mail: coalson@pitt.edu. Phone: (412)624-8261. Fax: (412)624-861.

Notes

The authors declare no competing financial interest.

[†]E-mail: hoc2@pitt.edu.

■ ACKNOWLEDGMENTS

We gratefully acknowledge financial support from the NSF grant CHE-0750332 and computational support from the National Science Foundation through TeraGrid resources (TG-MCB110137) and computational support from the Center for

Molecular and Materials Simulation (CMMS) at the University of Pittsburgh. TeraGrid systems are hosted by Indiana University, LONI, NCAR, NCSA, NICS, ORNL, PSC, Purdue University, SDSC, TACC, and UC/ANL.

■ REFERENCES

- (1) Lynch, J. W. *Physiol. Rev.* **2004**, *84*, 1051–1095.
- (2) Wotring, V. E.; Miller, T. S.; Weiss, D. S. *J. Physiol.* **2003**, *548*, 527–540.
- (3) Cymes, G. D.; Grosman, C. *Nature* **2011**, *474*, 526–530.
- (4) Hibbs, R. E.; Gouaux, E. *Nature* **2011**, *474*, 54–60.
- (5) Keramidas, A.; Moorhouse, A. J.; Pierce, K. D.; Schofield, P. R.; Barry, P. H. *J. Gen. Physiol.* **2002**, *119*, 393–410.
- (6) Keramidas, A.; Moorhouse, A. J.; Peter, P. R.; Barry, P. H. *Prog. Biophys. Mol. Biol.* **2004**, *86*, 161–204.
- (7) Sine, S. M.; Wang, H. L.; Hansen, S.; Taylor, P. *J. Mol. Neurosci.* **2010**, *40*, 70–76.
- (8) Hilf, R. J.; Dutzler, R. *Nature* **2009**, *457*, 115–118.
- (9) Bocquet, N.; Nury, H.; Baaden, M.; Le Poupon, C.; Changeux, J. P.; Delarue, M.; Corringer, P. J. *Nature* **2009**, *457*, 111–114.
- (10) Gonzalez-Gutierrez, G.; Grosman, C. *J. Mol. Biol.* **2010**, *403*, 693–705.
- (11) Parikh, R. B.; Bali, M.; Akabas, M. H. *J. Biol. Chem.* **2011**, *286*, 14098–14109.
- (12) Willenbring, D.; Liu, L.; Mowrey, D.; Xu, Y.; Tang, P. *Biophys. J.* **2011**, *101*, 1905–1912.
- (13) Nury, H.; Poitevin, F.; Van Renterghem, C.; Changeux, J. P.; Corringer, P. J.; Delarue, M.; Baaden, M. *Proc. Natl. Acad. Sci. U. S. A.* **2010**, *107*, 6275–6280.
- (14) Zhu, F.; Hummer, G. *Proc. Natl. Acad. Sci. U. S. A.* **2010**, *107*, 19814–19819.
- (15) Suhre, K.; Sanejouand, Y. H. *Nucleic Acids Res.* **2004**, *32*, W610–614.
- (16) Taly, A.; Delarue, M.; Grutter, T.; Nilges, M.; Le Novere, N.; Corringer, P. J.; Changeux, J. P. *Biophys. J.* **2005**, *88*, 3954–3965.
- (17) Szarecka, A.; Xu, Y.; Tang, P. *Proteins* **2007**, *68*, 948–960.
- (18) Haddadian, E. J.; Cheng, M. H.; Coalson, R. D.; Xu, Y.; Tang, P. *J. Phys. Chem. B* **2008**, *112*, 13981–13990.
- (19) Taly, A.; Corringer, P. J.; Grutter, T.; Prado de Carvalho, L.; Karplus, M.; Changeux, J. P. *Proc. Natl. Acad. Sci. U. S. A.* **2006**, *103*, 16965–16970.
- (20) MacKerell, A. D.; Bashford, D.; Bellott, M.; Dunbrack, R. L.; Evanseck, J. D.; Field, M. J.; Fischer, S.; Gao, J.; Guo, H.; Ha, S.; et al. *J. Phys. Chem. B* **1998**, *102*, 3586–3616.
- (21) Li, H.; Robertson, A. D.; Jensen, J. H. *Proteins* **2005**, *61*, 704–721.
- (22) Phillips, J. C.; Braun, R.; Wang, W.; Gumbart, J.; Tajkhorshid, E.; Villa, E.; Chipot, C.; Skeel, R. D.; Kale, L.; Schulten, K. *J. Comput. Chem.* **2005**, *26*, 1781–1802.
- (23) Mackerell, A. D., Jr.; Feig, M.; Brooks, C. L., 3rd. *J. Comput. Chem.* **2004**, *25*, 1400–1415.
- (24) Darden, T.; York, D.; Pedersen, L. *J. Chem. Phys.* **1993**, *98*, 10089–10092.
- (25) Graf, P.; Nitzan, A.; Kurnikova, M. G.; Coalson, R. D. *J. Phys. Chem. B* **2000**, *104*, 12324–12338.
- (26) Cheng, M. H.; Coalson, R. D.; Tang, P. *J. Am. Chem. Soc.* **2010**, *132*, 16442–16449.
- (27) Cheng, M. H.; Cascio, M.; Coalson, R. D. *Biophys. J.* **2005**, *89*, 1669–1680.
- (28) Kurnikova, M. G.; Coalson, R. D.; Graf, P.; Nitzan, A. *Biophys. J.* **1999**, *76*, 642–656.
- (29) Cheng, M. H.; Coalson, R. D. *J. Phys. Chem. B* **2005**, *109*, 488–498.
- (30) Ermak, D. L.; McCammon, J. A. *J. Chem. Phys.* **1978**, *69*, 1352–1360.
- (31) Hille, B. *Ion channels of excitable membranes*, 3rd ed.; Sinauer Associates, Inc.: Sunderland, MA, 2001.
- (32) Darve, E.; Rodriguez-Gomez, D.; Pohorille, A. *J. Chem. Phys.* **2008**, *128*, 144120–144133.
- (33) Chipot, C.; Hénin, J. *J. Chem. Phys.* **2005**, *123*, 244906–244912.
- (34) Ivanov, I.; Cheng, X.; Sine, S. M.; McCammon, J. A. *J. Am. Chem. Soc.* **2007**, *129*, 8217–8224.
- (35) Smart, O. S.; Neduvilil, J. G.; Wang, X.; Wallace, B. A.; Sansom, M. S. *J. Mol. Graph.* **1996**, *14*, 354–360, 376.
- (36) Humphrey, W.; Dalke, A.; Schulten, K. *J. Mol. Graph.* **1996**, *14*, 33–38.
- (37) Cheng, X.; Ivanov, I.; Wang, H.; Sine, S. M.; McCammon, J. A. *Biophys. J.* **2007**, *93*, 2622–2634.
- (38) Zimmermann, I.; Dutzler, R. *PLoS Biol.* **2011**, *9*, e1001101.
- (39) Keramidas, A.; Moorhouse, A. J.; French, C. R.; Schofield, P. R.; Barry, P. H. *Biophys. J.* **2000**, *79*, 247–259.
- (40) Lynch, J. W.; Rajendra, S.; Pierce, K. D.; Handford, C. A.; Barry, P. H.; Schofield, P. R. *EMBO J.* **1997**, *16*, 110–120.
- (41) Sunesen, M.; de Carvalho, L. P.; Dufresne, V.; Grailhe, R.; Savatier-Duclert, N.; Gibor, G.; Peretz, A.; Attali, B.; Changeux, J. P.; Paas, Y. *J. Biol. Chem.* **2006**, *281*, 14875–14881.
- (42) Cheng, M. H.; Cascio, M.; Coalson, R. D. *Proteins: Struct., Funct., Bioinf.* **2007**, *68*, 581–593.
- (43) Miyazawa, A.; Fujiiyoshi, Y.; Unwin, N. *Nature* **2003**, *423*, 949–955.
- (44) Bahar, I.; Lezon, T. R.; Yang, L.-W.; Eyal, E. *Annu. Rev. Biophys.* **2010**, *39*, 23–42.